Sensitivity of the Kurtosis Statistic as a Detector of Pulsed Sinusoidal RFI

Roger D. De Roo, *Member, IEEE*, Sidharth Misra, and Christopher S. Ruf, *Fellow, IEEE*

***Abstract*—A new type of microwave radiometer detector that is capable of identifying low-level pulsed radio frequency interference (RFI) has been developed. The Agile Digital Detector can discriminate between RFI and natural thermal emission signals by directly measuring other moments of the signal than the variance that is traditionally measured. The kurtosis is the ratio of the fourth central moment of the predetected voltage to the square of the second central moment. It can be an excellent indicator of the presence of RFI. A number of issues that are related to the proper calculation of the kurtosis are addressed. The mean and standard deviation of the kurtosis, in both the absence and the presence of pulsed sinusoidal RFI, are derived. The kurtosis is much more sensitive to short-pulsed RFI—such as from radars—than to continuous-wave RFI. The minimum detectable power for pulsed sinusoidal RFI is found to be proportional to $(M^3N)^{-1/4}$, where N is the number of independent samples and M is the number of frequency subbands in the receiver.**

***Index Terms*—Detectors, digital radio, interference suppression, microwave radiometry.**

I. Introduction

NUMEROUS studies have revealed that spaceborne microwave radiometers are subject to detrimental radio-frequency interference (RFI), particularly at the L- and C-bands [1]–[3] and also at the X-band [4], [5], and potentially at the K-band [6]. This RFI is insidious. The International Telecommunications Union (ITU) laments "that studies have established that measurements in absorption bands are extremely vulnerable to interference because, in general, there is no possibility to detect and to reject data that are contaminated by interference, and because propagation of undetected contaminated data into [numerical weather prediction] models may have a destructive impact on the reliability/quality of weather forecasting [7]." The ITU recommendation continues that the maximum interference level for spaceborne microwave radiometers in all bands should be one fifth of the power associated with the noise-equivalent brightness uncertainty (NEΔT) needed for the science objectives of the instrument. This recommendation is tight because RFI is additive, and therefore, random noise reduction techniques such as oversampling and averaging will be biased. While it is easy to remove large-amplitude RFI, for which contaminated measurements indicate physically implausible brightness, low-level RFI remains a problem. Since radiometers are themselves the most sensitive microwave receivers, the seriousness of the problem is not even known. This paper presents the theoretical basis behind a novel technique for detecting low-level RFI in radiometric observations.

Previous analog and digital signal-processing-based algorithms have been developed for RFI mitigation that are based on the detection of anomalous spikes in the power spectrum over narrow frequency bands [8], [9]. Such approaches will, in general, tend to have more trouble detecting low-level intermittent RFI. The Agile Digital Detector (ADD) is a digital signal-processing detector that uses an alternative approach to RFI detection and mitigation. High-order moments of the received signal are detected, from which characteristics of the probability distribution of its amplitude can be estimated. For a signal that is generated by thermal emission alone, the amplitude is Gaussian distributed. The presence of non-Gaussian-distributed RFI can be detected by its influence on the high-order moments. ADD performance has been empirically verified previously during ground-based field trials [10]. Presented here are statistical characteristics of ADD performance based on analytical considerations. The concept of kurtosis-based detection of RFI is first described in Section II. In Section III, the behavior of the kurtosis statistic in the absence of RFI is described. In Section IV, the behavior of the kurtosis statistic in the presence of pulsed sinusoidal RFI is introduced. A blind spot in the RFI detection algorithm and the threshold for RFI detectability are discussed in Section V.

For the purpose of illustrating by example some of the statistical concepts presented in this paper, it is useful to consider some relevant radiometer operating characteristics. We use values for the ADD prototype radiometer described in [10]. This radiometer operates with a 24-MHz total bandwidth that is divided into eight subbands, each 3 MHz wide, using digital filters. Data samples were taken with integration times of 36 ms. This yields the number of independent samples: $N = B\tau = 108\,000$ per observation in each subband. The system noise temperature $T_{\rm sys}$ of the radiometer was approximately 600 K while observing an ambient blackbody brightness temperature of 290 K. Radiometer gain was set so that the ADD digitizer covered a dynamic range of approximately six times the standard deviation of the Gaussian-distributed signal when $T_{\rm sys} = 600$ K. For interference sources, we consider the Air Route Surveillance Radars (ARSRs) operated by the U.S. Federal

Manuscript received May 25, 2006; revised August 28, 2006.This work was supported in part by the NASA Goddard Space Flight Center and its Earth Science Technology Office under Grant NNG05GB08G and Grant NNG05GL97G and in part by the NASA SBIR Program under Contract NNG05CA50C.

R. D. De Roo is with the Department of Atmospheric, Oceanic, and Space Sciences, University of Michigan, Ann Arbor, MI 48109 USA.

S. Misra was with the Space Physics Research Laboratory, University of Michigan, Ann Arbor, MI 48109 USA. He is now with the Danish National Space Center, Technical University of Denmark, 2800 Lyngby, Denmark.

C. S. Ruf is with the Space Physics Research Laboratory, University of Michigan, Ann Arbor, MI 48109 USA.

Digital Object Identifier 10.1109/TGRS.2006.888101

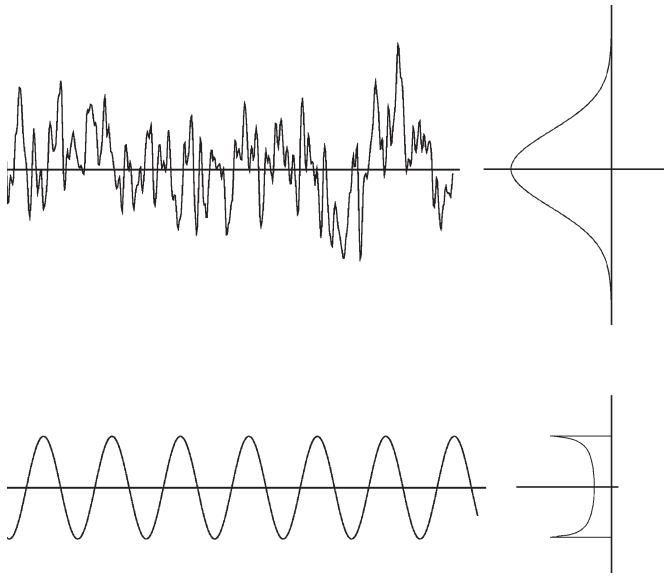

Fig. 1. Example of predetection signals. On the left are time-domain representations of the signals. Their pdfs are shown on the right. Geophysical signals and receiver noise are Gaussian distributed in amplitude (top), while sinusoids have a distinctly non-Gaussian pdf (bottom).

Aviation Administration. These L-band radars are distributed throughout the U.S. and transmit at megawatt peak power levels with center frequencies that range from 1215–1380 MHz [11], which is very close to the L-band passive band in the range of 1400–1427 MHz. ARSR-1 radars transmit with a 0.072% duty cycle, while ARSR-4 radars transmit with a 1%–3.24% duty cycle.

II. Principle of Kurtosis-Based RFI Detection in Microwave Radiometry

The signal detected by a microwave radiometer is primarily from natural thermal emission as well as thermal noise generated by the hardware. The probability density function (pdf) of the amplitude of this signal is Gaussian distributed. The most likely form of RFI is sinusoidal, which has a completely different amplitude distribution, as shown in Fig. 1.

In the absence of RFI, the random voltage v at the input to a digitizer is given by the Gaussian probability density $p_g(v)$, i.e.,

$$p_g(v) = \frac{1}{\sigma\sqrt{2\pi}} e^{\frac{-v^2}{2\sigma^2}}. \tag{1}$$

The RFI detection algorithm makes use of the higher order moments of the random variable v. The central moments of the distribution are given by

$$m_n^g = \langle (v - \langle v \rangle)^n \rangle = 1 \cdot 3 \cdot \cdots \cdot (n-1)\sigma^n \tag{2}$$

where σ is the standard deviation of v and n is even. The moment $m_n = 0$ when n is odd. In case of a Gaussian-distributed signal, higher order moments are uniquely determined by the standard deviation. The kurtosis of v is defined as

$$R = \frac{m_4}{m_2^2}. \tag{3}$$

For a Gaussian-distributed signal, the kurtosis is equal to 3, independent of σ. In case the signal is corrupted by RFI, the probability may deviate from a Gaussian distribution, and the value of the kurtosis may deviate from 3.

The detection of RFI thus reduces to the problem of deciding from its samples if a variable is normally distributed. This is a well-documented area of research [12]. The moment-ratio-based methods are especially appealing for radiometric operation because calculations of the test statistic are simple (and therefore fast), they do not require significant data storage (e.g., no ranking of data is required), and the postdetect data transmission rate is not significantly different from current receiver technologies that do not employ RFI detection. In addition, the statistic R is independent of the statistic m_2 for a Gaussian distribution [12]. Therefore, estimates of m_2 and hence of the brightness temperature will be unbiased by the removal of samples incorrectly flagged as containing RFI by a kurtosis-based algorithm. RFI detection algorithms which rely on brightness thresholds may be biased because high outliers are suppressed.

III. Kurtosis in the Absence of RFI

While the kurtosis is ideally equal to 3 for a Gaussian distribution, the measurement process results in a sample estimate of the kurtosis that can deviate from the theoretical value. This section explores some mechanisms of the measurement process and how they can affect the estimate of the kurtosis when no RFI is present.

A. Effects of Finite Number of Independent Samples

Because the kurtosis is estimated from a finite sample set, it is itself a random variable. Let its pdf be denoted by $p(R; N)$, where N is the number of independent samples. The area under the outlying tails of the pdf determines the rate of false detections of RFI in otherwise RFI-free radiometric observations. Closed-form expressions for $p(R; N)$ exist only for $N = 4$ [13], which is a sample size that is much too small for practical utility. Fortunately, the moments of $p(R; N)$ are known exactly for arbitrary N up to the seventh moment [14]–[16] and can be used to estimate the area under its tails. In the limit of large N, $p(R; N)$ tends toward normal with mean $\langle R \rangle = 3(N-1)/(N+1)$ and variance that asymptotically approaches $24/N$. The normal approximation requires a rather large N ($N > 50\,000$). For radiometer applications with very fine bandwidth resolution and very short integration times, the non-Gaussian nature of $p(R; N)$ should be taken into account in order to minimize the false alarms of RFI detection.

A common moment-based estimator for pdfs and cumulative distribution functions (CDFs) is the Edgeworth series [17], but this series generates negative values for the pdf in the tails, resulting in poor area estimates under the tails. Bowman

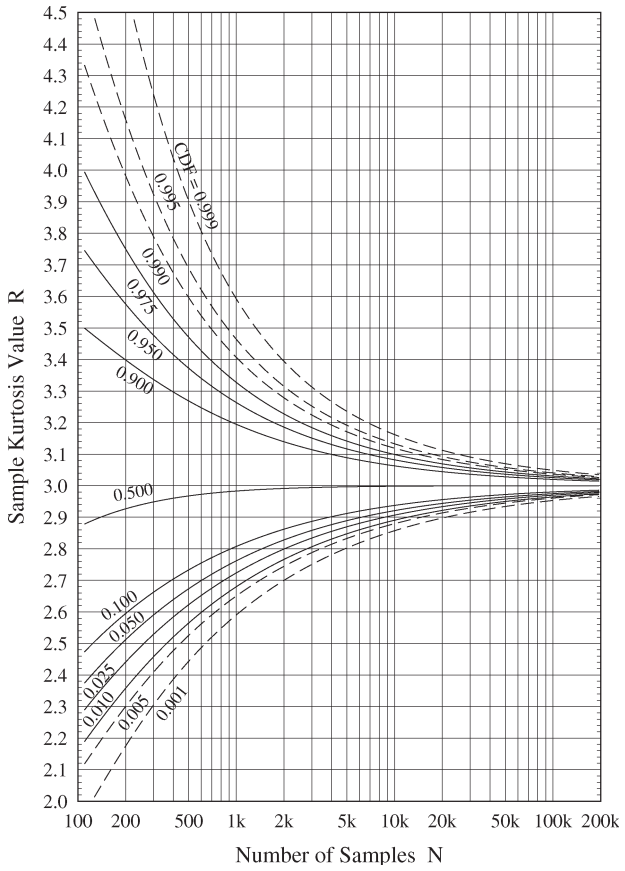

Fig. 2. Contours of the CDF for the kurtosis R as a function of the number of independent samples N when the samples are drawn from a Gaussian population.

and Shenton [18] recommend an alternative approximation for $N > 25$ given by

$$p(R;N) = \frac{1}{\sqrt{2\pi}} \exp\left(-\frac{1}{2}\left(\gamma + \delta \sinh^{-1}\left(\frac{R-\xi}{\lambda}\right)\right)^2\right) \times \frac{\delta}{\sqrt{(R-\xi)^2+\lambda^2}} \quad (4)$$

where the parameters γ, δ, λ, ξ are estimated from the first four moments of $p(R;N)$ using the algorithm of [19]. The contours of constant CDF, which are calculated with this method, are shown in Fig. 2. This plot extends from sufficiently low N ($\sim$100) that comparisons can be made to other approximations, such as the empirically derived curves for $20 < N < 200$ in [20], with which they agree quite closely, except far out on the tails (for the CDF < 0.007 and CDF > 0.975 curves). Out on the tails for these low values of N, the curves in Fig. 2 are slightly conservative. Above approximately $N = 50\,000$, the distribution of R can be described as normal, but at fewer samples, the tail for large R is longer than the tail for small R, and different thresholds for departures from 3 should be considered for the upper and lower tails to flag the presence of RFI. To take an extreme example, at $N = 2000$, a blind application of the large N limit of the variance would indicate that the symmetric 1% thresholds, namely, the mean ± 2.58 standard deviations, for RFI-free R should be $2.715 < R < 3.279$. While the RFI-free rejection is about the same (1.1%), the actual 1% thresholds are $2.744 < R < 3.315$. As will be seen here, this offset of the correct thresholds strengthens the moment-ratio test against continuous-wave (CW) RFI, but it weakens it against short-pulsed RFI.

TABLE I
RATIO OF SAMPLES WITHIN THE DIGITIZER SPAN TO OUTLIERS FOR AN RFI-FREE SIGNAL WITH DIFFERENT DIGITIZER SPANS

ADC span	Odds against an outlier
± σ	2.15 : 1
± 2σ	21 : 1
± 3σ	369 : 1
± 4σ	15.8 k : 1
± 5σ	1.74 M : 1
± 6σ	506 M : 1

B. Effects of Clipping by Digitizers

All digitizers have a finite input range. For the moment-ratio method to work properly, out-of-range signals must be sufficiently rare so as not to appreciably disturb the expected statistics of the RFI-free data. This can easily be achieved since the tails of the Gaussian pdf fall off very rapidly. Table I gives the ratio of the area below the Gaussian curve within specified limits to the area outside those limits. This is equivalent to the ratio of the number of samples within the limits to those that fall outside of them or the odds against an outlier. Even for very modest spans, keeping the expected number of outliers below 1 per integration period can be easily achieved. Sufficient span is also important to prevent clipping of RFI since the easiest RFI to detect is that which is very strong.

C. Effects of Digitizer Null Offset

There has been no distinction thus far between the moments about the origin μ_n and the moments about the mean m_n because all RF signals have zero mean. However, the digitizing hardware often introduces a mean into the data because the analog-to-digital converter (ADC) has a null offset. In terms of the digitizer outputs v_i, the nth moment about the origin is given by

$$\mu_n = \frac{1}{N_s}\sum_{i=1}^{N_s} v_i^n \quad (5)$$

where N_s is the number of digitized samples, f_s is the sampling rate, τ is the integration time, and $N_s = 1 + f_s\tau$. Since the digitizing rate may exceed the bandwidth of the signal, the samples may be correlated, and the number of digitized samples N_s may exceed the number of independent samples N. However, the number of independent samples cannot exceed the number of samples collected. In other words, $N_s \geq N$, with the equality holding when $f_s \leq B$. The moment about the origin calculations is very easily achieved for even rather rapid sampling rates in digital logic such as a field-programmable gate array (FPGA). The moments about the mean as a function

of the moments about the origin can be readily derived with the binomial formula [21]

$$m_2^a = \mu_2 - \mu_1^2 \tag{6}$$

$$m_4^a = \mu_4 - 4\mu_3\mu_1 + 6\mu_2\mu_1^2 - 3\mu_1^4 \tag{7}$$

where the superscript a indicates an ideal analog operation, i.e., without the effects of digitization. Thus, a digital receiver configured to perform kurtosis calculations should collect the first four moments about the origin of the data to correct for the ADC null offset. Null offsets of even a fraction of a digitizing bin can be removed in this manner.

D. Effects of Digitization

Digitization of the signal results in a small loss of information since the continuous random variable is binned by the ADC. For example, the variance of a digitized Gaussian signal is larger than the variance of the analog signal by the variance of a uniform distribution that is one digitizing bin wide. This is because the act of digitizing can be viewed as adding to the analog signal a random amount, which is either positive or negative up to one half of a digitizing bin. If the signal strength is sufficiently strong, the amount added to the data by digitization is nearly uniformly distributed. A similar effect occurs to all even moments of a digitized distribution. Fischman and England [22] have derived the effects of digitization on the moments of a Gaussian distribution as a function of the width of a digitization bin v_0. They found that

$$m_2^d = \sigma^2 + \frac{1}{12}v_0^2 \tag{8}$$

$$m_4^d = 3\sigma^4 + \frac{1}{2}\sigma^2 v_0^2 + \frac{1}{80}v_0^4 \tag{9}$$

where the superscript d indicates that the Gaussian signal has been digitized. They further found that the correction for the variance is accurate for a Gaussian signal as long as the standard deviation σ is greater than $2/3\ v_0$ and the correction for the fourth moment is accurate for $\sigma > 3/4\ v_0$.

For radio brightness measurements of the second moment, this digitization offset is a constant and can be lumped with the receiver temperature. For kurtosis measurements of thermal noise, the digitization offsets in the second and fourth moments nearly cancel when the ratio (3) is taken, i.e.,

$$\frac{m_4^d}{\left(m_2^d\right)^2} = 3 - \frac{\frac{1}{120}}{\left(\left(\frac{\sigma}{v_0}\right)^2 + \frac{1}{12}\right)^2}. \tag{10}$$

The offset induced in the kurtosis statistic by neglecting the effects of digitization is always negative, and while it is about -1% at $\sigma = 2/3\ v_0$, it decreases to -0.24% at $\sigma = v_0$ and decreases further as the signal strength at the ADC input is increased. For the case of the ADD measurements presented in [10], the instrument gain was set so that $\sigma = 10v_0$.

The correction for the effects of digitization has been derived by Sheppard and is given by [21]

$$\begin{aligned} m_2 &= \mu_2 - \mu_1^2 - \frac{1}{12}v_0^2 \\ m_4 &= \mu_4 - 4\mu_3\mu_1 + 6\mu_2\mu_1^2 - 3\mu_1^4 \\ &\quad - \frac{1}{2}\left(\mu_2 - \mu_1^2\right)v_0^2 + \frac{7}{240}v_0^4. \end{aligned} \tag{11}$$

These moments are the estimators of the second and fourth central moments, which are unbiased by the effects of digitization, in terms of the output of the FPGA. Errors in the ADC transfer function measured by the differential and integral nonlinearities have not been considered. While radiometric and even interferometric operation is quite feasible with only a few levels, Sheppard's correction must be generalized for optimal signal detection [23]. In the rest of this paper, our measurements were made with sufficiently strong signals that Sheppard's correction has been neglected.

IV. Kurtosis in the Presence of Pulsed Sinusoidal RFI

The kurtosis may change in the presence of RFI. Here, we characterize the behavior of the kurtosis in the presence of a radarlike source of RFI.

A. Combined Gaussian Noise and a Pulsed Sinusoid

Assume that the RFI can be modeled as a pulsed sinusoid with an amplitude A and total duration $d\tau$, where τ is the radiometer integration time and $0 \le d \le 1$. In our case, even though the RFI is deterministic in nature, we consider its amplitude histogram as an equivalent probability distribution. The pdf of such a waveform is given by

$$p_{\mathrm{ps}}(v) = (1-d)\delta(v) + \frac{d}{\pi\sqrt{A^2 - v^2}} \tag{12}$$

where $\delta(x)$ is the Dirac delta function. If the integration time greatly exceeds the interpulse period, then d is the radar's duty cycle, which is the proportion of time that the radar is transmitting. We require the probability distribution of the combined signal that includes both thermal emission and the RFI signal. Rice [24] determined the probability distribution function for the instantaneous voltage of a sinusoid with noise, which is easily extended to the case of a pulsed sinusoid, i.e.,

$$p(v) = \frac{1}{\sqrt{2\pi}\sigma}e^{\frac{-v^2}{2\sigma^2}}\left(1 + d\sum_{k=1}^{\infty}\frac{1}{(k!)^2}\left(\frac{A}{2\sigma}\right)^{2k}He_{2k}\left(\frac{v}{\sigma}\right)\right) \tag{13}$$

where

$$He_{2k}(x) = \sum_{m=0}^{k}\frac{(-1)^m}{2^m}\frac{(2k)!}{m!(2k-2m)!}x^{2k-2m} \tag{14}$$

is a Hermite polynomial of even order [17]. When $d = 0$ or $A = 0$, the expression reduces to a Gaussian probability

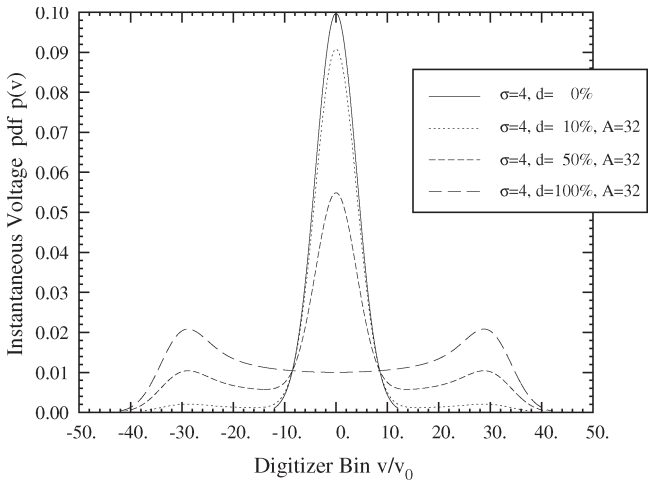

Fig. 3. Instantaneous voltage pdf for constant Gaussian noise level and constant pulsed sinusoid amplitude but varying duty cycle.

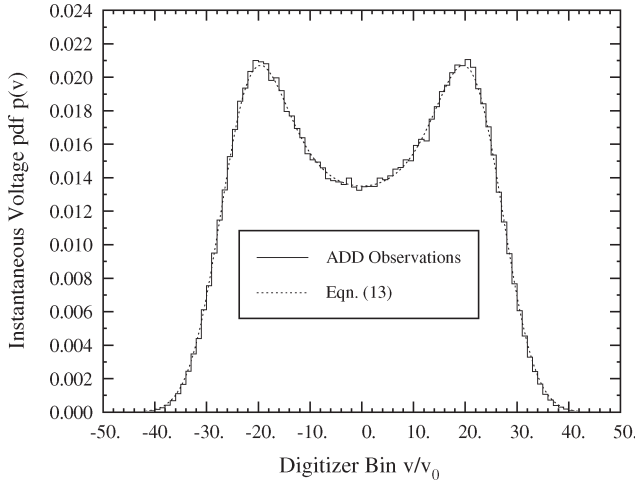

Fig. 4. Comparison of (13) with the ADD output while the radiometer is observing the sky with an equivalent of 2000 K of CW at 1412 MHz added to the input.

distribution. Rice's result is the case when $d = 1$. Fig. 3 shows the shapes predicted by (13) for constant noise and pulsed sinusoid amplitudes. Fig. 4 shows a comparison of Rice's result with the measurements presented in [10].

In order to calculate the statistical behavior of the kurtosis, we require the first four moments of the resultant signal. Since the distributions are symmetric about $v = 0$, the odd moments are zero. Thus, the first four nonzero moments for the signal with pulsed sinusoidal contamination become

$$m_2^{\rm ps} = \sigma^2 + \frac{dA^2}{2} = \sigma^2(1+S) \tag{15}$$

$$m_4^{\rm ps} = 3\left(\sigma^4 + dA^2\sigma^2 + \frac{dA^4}{8}\right) = 3\sigma^4\left(1 + 2S + \frac{1}{2d}S^2\right) \tag{16}$$

$$m_6^{\rm ps} = 5\sigma^6\left(3 + 9S + \frac{9}{2d}S^2 + \frac{2}{(2d)^2}S^3\right) \tag{17}$$

$$m_8^{\rm ps} = 35\sigma^8\left(3 + 12S + \frac{18}{2d}S^2 + \frac{8}{(2d)^2}S^3 + \frac{1}{(2d)^3}S^4\right) \tag{18}$$

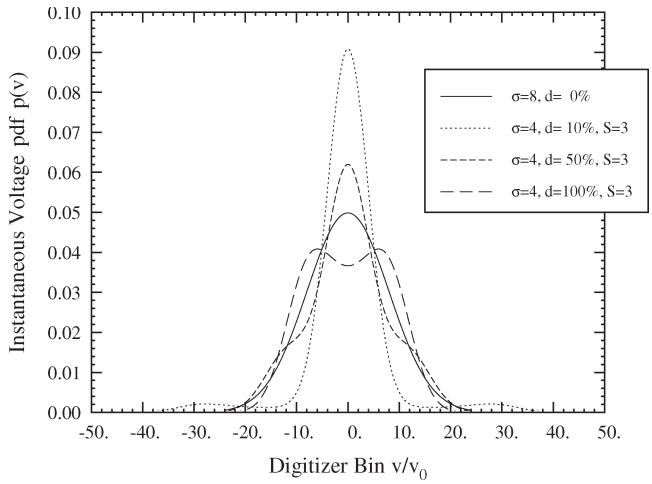

Fig. 5. Examples of instantaneous voltage pdfs with the same variance ($m_2^{\rm ps} = 64$). Pulsed sinusoidal RFI, when present, has a constant signal-to-noise power level but different duty cycles. The low-duty-cycle RFI has the highest tails and is easiest to detect with the kurtosis statistic.

where S is the signal-to-noise ratio of the pulsed sinusoid power ($P_{\rm ps} = dA^2/2$, which is averaged over an integration period) to the noise power and is given by

$$S = \frac{dA^2}{2\sigma^2} = \frac{P_{\rm ps}}{kT_{\rm sys}B} = \frac{T_{\rm ps}}{T_{\rm sys}} \tag{19}$$

where $\sigma^2 = kT_{\rm sys}B$, k is the Boltzmann constant, and B is the RF bandwidth. S is also the ratio of the equivalent RFI brightness temperature $T_{\rm ps}$ to the system temperature (in the absence of RFI) $T_{\rm sys}$. The shape of the pdf of the instantaneous voltage as a function of the duty cycle, but with the total power kept constant, is depicted in Fig. 5. The tails of the distribution are highest at low duty cycles.

B. Mean and Variance of Kurtosis With Pulsed Sinusoidal RFI

In the presence of pulsed sinusoidal RFI, the large sample expected value of the kurtosis becomes

$$\overline{R}(S,d) = \frac{m_4^{\rm ps}}{(m_2^{\rm ps})^2} = 3\frac{\left(1 + 2S + \frac{1}{2d}S^2\right)}{(1+S)^2}. \tag{20}$$

In the CW limit ($d = 1$), $\overline{R}$ ranges from 3 to 3/2 as the power in the sinusoid increases. However, as $d \to 0$ but $S > 0$ (corresponding to very short radar pulses), $\overline{R} > 3$. These departures from 3 enable the detection of RFI.

The large sample variance in the kurtosis statistic can be derived from the moments to be [25]

$$\sigma_R^2(S,d) = \frac{1}{N\left(m_2^{\rm ps}\right)^4} \times \left[m_8^{\rm ps} - \left(m_4^{\rm ps}\right)^2 + \frac{4\left(m_4^{\rm ps}\right)^3}{\left(m_2^{\rm ps}\right)^2} - \frac{4m_4^{\rm ps}m_6^{\rm ps}}{m_2^{\rm ps}}\right]. \tag{21}$$

For $S = 0$ (i.e., in the absence of RFI), the variance of the kurtosis statistic reduces to $\sigma_R^2(S=0) = 24/N$. We shall denote this special value as σ_{R0}^2.

V. Limits of Detection

A. Blind Spot and False Alarm Rate (FAR)

If the kurtosis becomes 3, then, in spite of the presence of RFI, the algorithm will fail to detect it. This indicates a blind spot in the algorithm. Two conditions are possible in which the kurtosis becomes 3: $S = 0$ or $d = 1/2$. The first condition corresponds to the absence of RFI, while the second is an algorithm blind spot. It is worth noting that practical radars tend to operate with duty cycles well below 50%, and so radiometers will generally not be subject to this problem. Nonetheless, this result is somewhat surprising given the obvious differences between the 50% duty cycle and Gaussian pdfs in Fig. 5. This is because the kurtosis is just one more parameter that describes the pdf. A more complete description of the pdf requires more moments of the pdf.

In light of the variance in R even in the absence of RFI, there will be a range of RFI around $R = 3 \pm z\sigma_{R0}$ for some z determined by the desired FAR for which the kurtosis algorithm is blind. To determine this region of blindness, we solve (20) for the duty cycle, i.e.,

$$d = \frac{\frac{3}{2}S^2}{(1+S)^2 R - 3(1+2S)}. \tag{22}$$

Provided that the number of independent samples N is sufficiently high to invoke the normal distribution of the kurtosis R, the relation between a specified FAR and the threshold values of the kurtosis $R_{\rm tha} = 3 + z_a\sigma_{R0}$ and $R_{\rm thb} = 3 - z_b\sigma_{R0}$ is given by $\text{FAR} = \text{FAR}_a + \text{FAR}_b$, where

$$\text{FAR}_{a,b} = \frac{1}{2}\left(1 - \text{erf}(z_{a,b}/\sqrt{2})\right) \tag{23}$$

and the subscripts a and b refer to the tail of the distribution "above" and "below" the RFI-free kurtosis mean value of 3.

Fig. 6 illustrates the region of sinusoid amplitude and duty cycle in which the signal will not be detected by the kurtosis for a given number of independent samples and FAR. The kurtosis is blind at a 50% duty cycle. In this example, the FAR is nearly symmetric ($\text{FAR}_a = \text{FAR}_b$) because N is sufficiently large to invoke the normal distribution of R and $z = z_a = z_b$. For the curves presented in Fig. 6, $z\sigma_{R0} = 0.03$, which corresponds to an arbitrarily chosen $\text{FAR} = 4.4\%$ for $N = 108\,000$. Under these conditions, the 100% duty cycle (CW) limit of detection is $S = -7.84$ dB, corresponding to $T_{\rm ps} = 99$ K, assuming an RFI-free $T_{\rm sys} = 600$ K. The limit of detection for very short duty cycle RFI is lower. For example, the $\sim$1% duty cycle of ARSR-4 radars should be detectable at -18.4 dB (8.3 K), and the $\sim$0.1% duty cycle of ARSR-1 radars should be detectable at $S = -23.4$ dB (2.7 K) at $\text{FAR} = 4.4\%$. For $\text{FAR}_a = 10\%$, the ARSR-1 detectable limit is $S = -24.4$ dB (2.2 K). This is very close to the ideal radiometric uncertainty since $\text{NE}\Delta\text{T} = T_{\rm sys}/\sqrt{N} = 1.8$ K.

B. Probability of Detection

When the number of samples N is sufficiently large to describe the distribution of the kurtosis as having a Gaussian distribution with mean $\overline{R}$ and standard deviation σ_R, we can predict not only the FAR but also the probability of detection (PD) for a given threshold value of kurtosis $R_{\rm th}$, strength S, and duty cycle d of pulsed sinusoid RFI. Considering the blind spot at $d = 1/2$, the PD for RFI with $d < 1/2$ (e.g., radars) will be denoted as PD_a because we expect R to be above 3, while RFI with $d > 1/2$ (e.g., CW RFI) will be denoted as PD_b because we expect R to be below 3. These probabilities of detection are given as

$$\text{PD}_{a,b} = \frac{1}{2}\left(1 \mp \text{erf}\left(\left(R_{\text{tha},b} - \overline{R}(S,d)\right)/\sqrt{2}\sigma_R(S,d)\right)\right). \tag{24}$$

Figs. 7 and 8 show the receiver operating characteristic charts for 0.1% and 1% duty cycles, respectively, while Fig. 9 shows the same for 100% duty cycle, for a fixed $N = 108\,000$. The performance of the algorithm is much better at a low duty cycle.

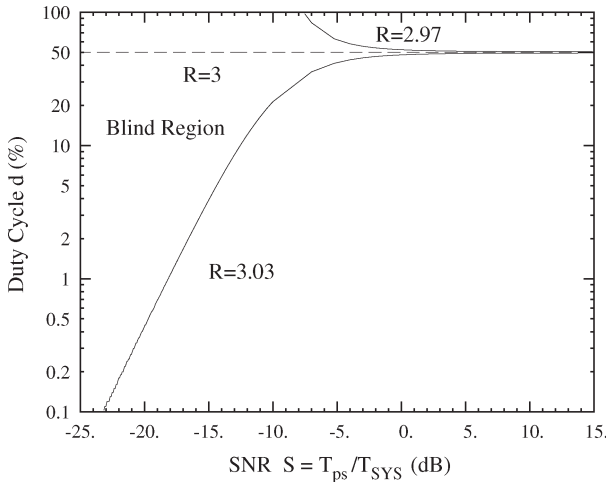

Fig. 6. Kurtosis blindness to pulsed sinusoidal RFI, with $z\sigma_{R0} = 0.03$, which is the 4.4% FAR for $B\tau = 108\,000$. The pulsed sinusoidal RFI with duty cycle and power between the $R = 3 \pm z\sigma_{R0}$ curves are not detectable. At any power level, a 50% duty cycle is undetectable. The limit of detectability for very short pulsed RFI is much lower than that for CW RFI and approaches NEΔT.

C. Dependence of Detection of RFI on System Parameters

For a duty cycle d that is small, the sinusoid amplitude A must be substantial to obtain a particular level of interference. The digitizer must not clip this short duration pulse, or we will effectively reduce the interference to the point where it remains present but is not detectable. If we arbitrarily consider the minimum $T_{\rm ps}$ which is unambiguously detectable without using the kurtosis statistic as being equal to, say, 10NEΔT, then the digitizer should not clip the signal for $S < 10/\sqrt{N}$. Solving the first equality of (19) for the sinusoid amplitude, we obtain $A = 7.8\,\sigma$ when $d = 0.1\%$ and $N = 108\,000$. This implies the ADC should have about three bits more than it needs to digitize the RFI-free radiometric signal.

If we are to fix the FAR and PD, we can determine the minimum detectable pulsed sinusoidal RFI using the kurtosis statistic. Consider, as a representative detection situation,

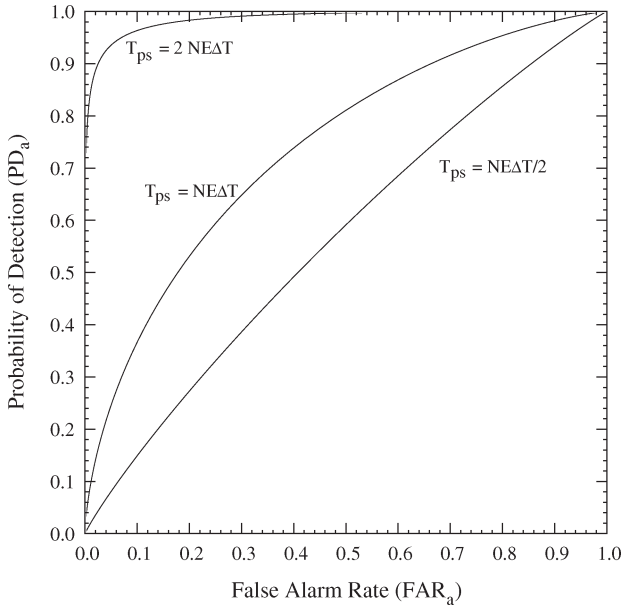

Fig. 7. Probability of detection of a pulsed sinusoid with 0.1% duty cycle versus single-sided FAR. $N = 108\,000$. At an RFI contribution equal to 2NEΔT, detection exceeds 90% for a FAR of 3%.

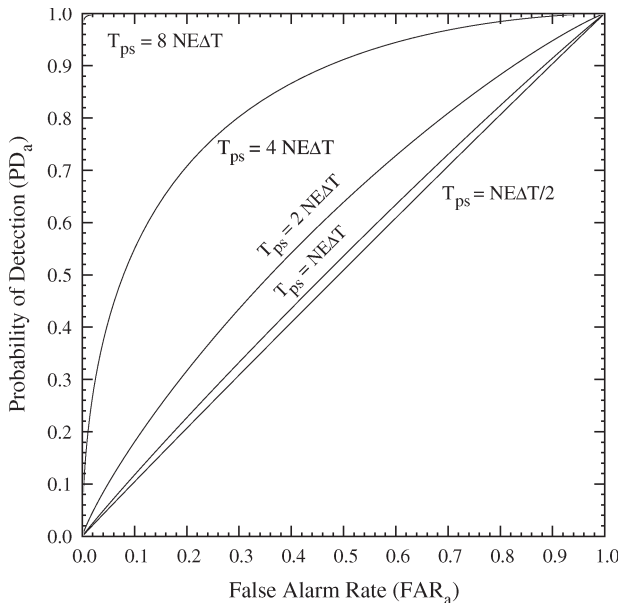

Fig. 8. Probability of detection of a pulsed sinusoid with 1% duty cycle versus single-sided FAR. $N = 108\,000$. The detection of RFI at a strength of 8NEΔT is nearly perfect.

setting the PD to PD $= 1 -$ FAR. This is equivalent to setting the threshold kurtosis value to the same number of standard deviations away from the means of both the RFI-free and pulsed sinusoidal RFI-containing pdfs, i.e.,

$$R_{\mathrm{tha},b} = 3 - z\sigma_{R0} = \overline{R}(S_{\min}, d) + z\sigma_R(S_{\min}, d) \qquad (25)$$

where $S_{\min}$ is the minimum detectable S and z is a parameter that is fixed based on the desired FAR. For example, FAR$_{b,a} = 15.87\%$ for $z = \pm 1$, FAR$_{b,a} = 2.28\%$ for $z = \pm 2$,

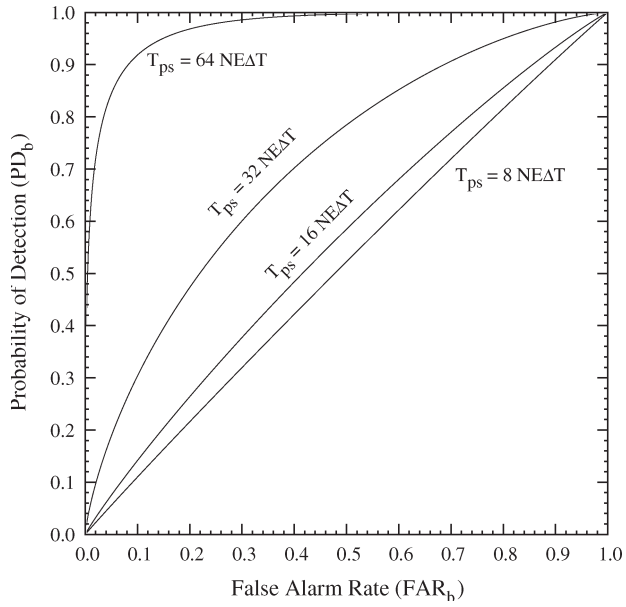

Fig. 9. Probability of detection of a CW tone (duty cycle of 100%) versus single-sided FAR. $N = 108\,000$. The power in the sinusoid must get relatively strong to be reliably detected in a single look.

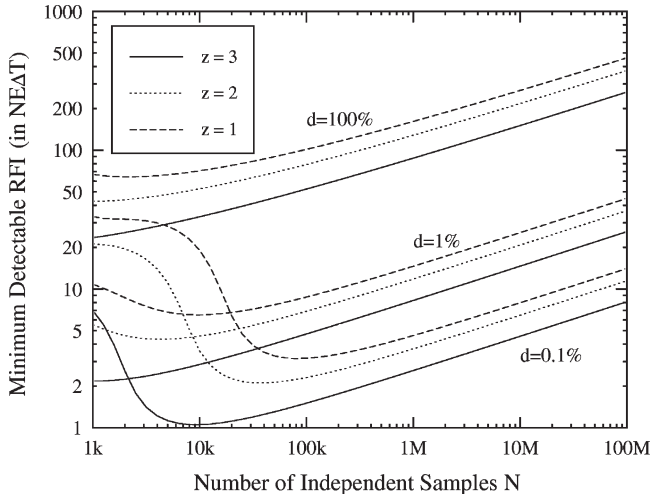

Fig. 10. Minimum detectable RFI as a function of the number of samples N and duty cycle d for a fixed FAR and PD, with PD $= 1 -$ FAR, and the FAR determined by the threshold kurtosis $R_{\mathrm{th}} = 3 \pm z\sigma_{R0}$. For $N >$ 100 000, the kurtosis algorithm is most sensitive to short duty cycle RFI. The minimum detectable RFI, when measured in Kelvin, is proportional to $N^{-1/4}$ for a large N.

and FAR$_{b,a} = 0.13\%$ for $z = \pm 3$. Solving the equation for the constant z, we get

$$z = \frac{3S_{\min}^2\sqrt{\frac{N}{24}}\left(1 - \frac{1}{2d}\right)}{(1 + S_{\min})^2\left(1 + \sigma_R(S_{\min}, d)/\sigma_{R0}\right)}. \qquad (26)$$

As $N \to \infty$, the ratio of the standard deviations becomes constant, and $S_{\min}$ is proportional to $N^{-1/4}$. Expressed in terms of the ideal radiometer uncertainty NEΔT, which itself is proportional to $N^{-1/2}$, the minimum detectable RFI grows as $N^{1/4}$, as shown in Fig. 10. Thus, the kurtosis algorithm can be used to detect an arbitrarily low level of RFI, but the number

of samples needed to do so increases somewhat faster than that needed for a particular radiometric resolution.

Division of the RF bandwidth B into subbands is an approach to salvage some observations when the RFI is narrowband and has been used to detect RFI by comparing the power in each subband [8], [9]. Polyphase filters [26] can be used in the FPGA to divide the RF bandwidth into M subbands. This division into subbands also enhances the sensitivity of the kurtosis statistic to RFI. Because the RFI is presumed to be narrowband, the RFI signal strength for a subband with pulsed sinusoidal RFI is the same as that which would appear in the full reception bandwidth. However, the noise power is proportional to the bandwidth, and so the signal-to-noise ratio for the subband $S_{\rm sb}$ is enhanced by a factor of M over that of full bandwidth reception: $S_{\rm sb} = MS$. At the same time, the number of independent samples for each subband $N_{\rm sb}$ is reduced by a factor of M : $N_{\rm sb} = N/M$. Since the sensitivity analysis for one subband is the same as for full-band reception, we can conclude that $S_{\rm sb,min}$ is proportional to $N_{\rm sb}^{-1/4}$, or for the entire system, $S_{\rm min}$ is proportional to $(M^3N)^{-1/4}$. Thus, in terms of the minimum detectable RFI, the division of the received bandwidth into eight subbands, as done in the ADD, is equivalent to increasing the number of independent samples by a factor of 512 and reducing the minimum detectable RFI power by a factor of 4.75.

The limit of detection is a function of S, which is the ratio of the pulsed sinusoid power to the total Gaussian-distributed power. This Gaussian-distributed power is the system temperature $T_{\rm sys}$, which is the sum of the receiver noise temperature and the geophysical brightness temperature, which is the point of the radiometric observation, i.e., $T_{\rm sys} = T_{\rm REC} + T_B$. A reduction of the receiver noise figure, i.e., a reduction of $T_{\rm REC}$, is well known to reduce the standard error of observation of T_B. A quiet receiver also helps in the detection of RFI by reducing the $T_{\rm sys}$, the baseline from which the minimum detectible RFI power is calculated from the sinusoid to thermal power ratio S.

The standard error of the brightness observation can be reduced by combining observations together. The same can be done, at least in principle, to the other moments of the observation, thereby increasing the number of independent samples, and thus the sensitivity of the kurtosis test for RFI. However, much like the brightness uncertainty can increase for long integration times due to gain fluctuations or ultimately, scene brightness changes, the kurtosis is also sensitive to these effects. For example, if an RFI-free observation has a standard deviation σ_1 for a duration t_1 but then suddenly changes to σ_2 for a duration t_2, then $m_2 = (t_1\ \sigma_1^2 + t_2\ \sigma_2^2)/(t_1 + t_2)$, and $m_4 = 3(t_1\ \sigma_1^4 + t_2\ \sigma_2^4)/(t_1 + t_2)$. Thus

$$R = 3\frac{t_1^2\sigma_1^4 + t_1t_2\left(\sigma_1^4 + \sigma_2^4\right) + t_2^2\sigma_2^4}{t_1^2\sigma_1^4 + t_1t_2\left(2\sigma_1^2\sigma_2^2\right) + t_2^2\sigma_2^4}. \tag{27}$$

In this circumstance, $R = 3$ only if $\sigma_1 = \sigma_2$, $t_1 = 0$, or $t_2 = 0$, which are the conditions that correspond to a constant standard deviation. Otherwise, $R > 3$. Thus, integration periods should be restricted to limit the effects of gain and brightness changes on the kurtosis statistic as well as their effects on the brightness.

VI. Conclusion

The kurtosis of the predetected voltage has been presented as a means of detecting the presence of pulsed sinusoidal RFI in radiometric observations. The predetected voltage due to thermal emission obeys the Gaussian pdf, for which the kurtosis is 3, regardless of the variance (brightness) of the signal. Finite sample sizes, digitizer offsets, digitizer spans, and the digitizer bin size affect the kurtosis calculation in small but predictable ways in the absence of RFI. When pulsed sinusoidal RFI is added to the thermal noise, the kurtosis statistic can deviate significantly from 3, indicating the presence of the RFI. CW RFI tends to drive the kurtosis value to less than 3, while short duty cycle pulses, such as those from radars, drive the kurtosis to exceed 3. A pulsed sinusoid with a 50% duty cycle added to Gaussian noise has an expected kurtosis of 3 and thus cannot be detected by an RFI detection algorithm using the kurtosis. For very short duty cycle RFI, such as radar transmissions, the minimum RFI power for which the kurtosis can detect the RFI approaches the ideal radiometric uncertainty. The sensitivity of the kurtosis to RFI can be enhanced by dividing the system bandwidth in the receiver into multiple frequency subbands, possibly to the point that some RFI at the limit recommended by the ITU for spaceborne passive sensors is detectable. The ADD has been configured to use the RFI detection scheme based on the kurtosis of the predetected voltage. The ADD has been used in multiple campaigns to date, and the data collected is currently being processed to demonstrate the performance of the RFI detection scheme using the kurtosis.

References

[1] L. Li, E. G. Njoku, E. Im, P. Change, and K. S. Germain, "A preliminary survey of radio-frequency interference over the U.S. in Aqua AMSR-E data," *IEEE Trans. Geosci. Remote Sens.*, vol. 42, no. 2, pp. 380–390, Feb. 2004.

[2] E. G. Njoku, P. Ashcroft, T. K. Chan, and L. Li, "Global survey and statistics of radio-frequency interference in AMSR-E land observations," *IEEE Trans. Geosci. Remote Sens.*, vol. 43, no. 5, pp. 938–947, May 2005.

[3] D. M. Le Vine and M. Haken, "RFI at L-band in synthetic aperture radiometers," in *Proc. IGARSS*, Toulouse, France, Jul. 21–25, 2003, vol. 3, pp. 1742–1744.

[4] S. W. Ellingson and J. T. Johnson, "A polarimetric survey of radio-frequency interference in C- and X-bands in the continental United States using WindSat radiometry," *IEEE Trans. Geosci. Remote Sens.*, vol. 44, no. 3, pp. 540–549, Mar. 2003.

[5] L. Li, P. W. Gaiser, M. H. Bettenhausen, and W. Johnson, "WindSat radio-frequency interference signature and its identification over land and ocean," *IEEE Trans. Geosci. Remote Sens.*, vol. 44, no. 3, pp. 530–539, Mar. 2003.

[6] M. Younis, J. Maurer, J. Fortuny-Guasch, R. Schneider, W. Wiesbeck, and A. J. Gasiewski, "Interference from 24-GHz automotive radars to passive microwave Earth remote sensing satellites," *IEEE Trans. Geosci. Remote Sens.*, vol. 42, no. 7, pp. 1387–1389, Jul. 2003.

[7] International Telecommunications Union, *Interference Criteria for Satellite Passive Remote Sensing*, 2003, Geneva, Switzerland. ITU Recommendation ITU-R RS.1029-2.

[8] A. J. Gasiewski, M. Klein, A. Yevgrafov, and V. Leuski, "Interference mitigation in passive microwave radiometry," in *Proc. IGARSS*, Toronto, ON, Canada, 2002, vol. 3, pp. 1682–1684.

[9] J. T. Johnson, G. A. Hampson, and S. W. Ellingson, "Design and demonstration of an interference suppressing microwave radiometer," in *Proc. IGARSS*, Anchorage, AK, 2004, pp. 1683–1686.

[10] C. Ruf, S. M. Gross, and S. Misra, "RFI detection and mitigation for microwave radiometry with an agile digital detector," *IEEE Trans. Geosci. Remote Sens.*, vol. 44, no. 3, pp. 694–706, Mar. 2006.

[11] Federal Aviation Administration, *Spectrum Management Regulations and Procedures Manual*, FAA Order 6050.32A, May 1, 1998.
[12] R. B. D'Agostino and M. A. Stephens, *Goodness-of-Fit Techniques*. New York: Marcel Dekker, 1986.
[13] A. T. McKay, "The distribution of beta_2 in samples of 4 from a normal universe," *Biometrika*, vol. 25, no. 3/4, pp. 411–415, Dec. 1933.
[14] E. S. Pearson, "Note on tests for normality," *Biometrika*, vol. 22, no. 3/4, pp. 423–424, May 1931.
[15] C. T. Hsu and D. N. Lawley, "The derivation of the fifth and sixth moments of the distribution of b2 in samples from a normal population," *Biometrika*, vol. 31, no. 3/4, pp. 238–248, Mar. 1940.
[16] R. C. Geary and J. P. G. Worlledge, "On the computation of universal moments of tests of statistical normality derived from samples drawn at random from a normal universe," *Biometrika*, vol. 34, no. 1/2, pp. 98–110, Jan. 1947.
[17] M. Abramowitz and I. A. Stegun, *Handbook of Mathematical Functions*. Washington, DC: Nat. Bureau Standards, 1964.
[18] K. O. Bowman and L. R. Shenton, "Omnibus test contours for departures from normality based on sqrt(b1) and b2," *Biometrika*, vol. 62, no. 2, pp. 243–250, Aug. 1975.
[19] N. L. Johnson, "Tables to facilitate fitting S_U frequency curves," *Biometrika*, vol. 52, no. 3/4, pp. 547–558, 1965.
[20] R. B. D'Agostino and E. S. Pearson, "Tests for departures from normality. Empirical results for the distributions of b2 and sqrt(b1)," *Biometrika*, vol. 60, no. 3, pp. 613–622, Dec. 1973.
[21] S. Dawson, *An Introduction to the Computation of Statistics*. London, U.K.: Univ. London Press, 1933.
[22] M. A. Fischman and A. W. England, "Sensitivity of a 1.4 GHz direct-sampling digital radiometer," *IEEE Trans. Geosci. Remote Sens.*, vol. 37, no. 5, pp. 2172–2180, Sep. 1999.
[23] C. S. Ruf, "Digital correlators for synthetic aperture interferometric radiometry," *IEEE Trans. Geosci. Remote Sens.*, vol. 33, no. 5, pp. 1222–1229, Sep. 1995.
[24] S. O. Rice, "Statistical properties of a sine wave plus random noise," *Bell Syst. Tech. J.*, vol. 27, no. 1, pp. 109–157, Jan. 1948.
[25] M. G. Kendall, *Advanced Theory of Statistics*, 5th ed. New York: Hafner, 1952.
[26] F. J. Harris, *Multirate Signal Processing for Communication Systems*. Upper Saddle River, NJ: Prentice-Hall, 2004.

Roger D. De Roo (S'88–M'96) received the B.S. degree in letters and engineering from Calvin College, Grand Rapids, MI, in 1986, and the B.S.E., M.S.E., and Ph.D. degrees in electrical engineering from the University of Michigan, Ann Arbor, in 1986, 1989, and 1996, respectively. His dissertation topic was on the modeling and measurement of bistatic scattering of electromagnetic waves from rough dielectric surfaces.

From 1996 to 2000, he was a Research Fellow with the Radiation Laboratory, Department of Electrical Engineering and Computer Science, University of Michigan, where he investigated the modeling and simulation of millimeter-wave backscattering phenomenology of terrain at near grazing incidence. He is currently an Assistant Research Scientist with the Department of Atmospheric, Oceanic, and Space Sciences, University of Michigan. He has supervised the fabrication of numerous dual-polarization microcontroller-based microwave radiometers. His current research interests include digital correlating radiometer technology development and inversion of geophysical parameters such as soil moisture, snow wetness, and vegetation parameters from radar and radiometric signatures of terrain.

Sidharth Misra received the B.E. degree in electronics and communication from the Nirma Institute of Technology, Gujarat University, Ahmedabad, Gujarat, India, in 2004, and the M.S. degree in electrical engineering and computer science-signal processing from the University of Michigan, Ann Arbor, in 2006.

He was a Research Engineer with the Space Physics Research Laboratory, University of Michigan, where he worked on the analysis and implementation of the Agile Digital Detector for RFI mitigation. He has also worked on Oceansat-II for the Space Application Center, Indian Space Research Organization, Ahmedabad, India. He is currently a Research Assistant with the Danish National Space Center, Technical University of Denmark (DTU), Lyngby. He is also currently involved with RFI analysis for CoSMOS, an airborne campaign preparing for SMOS at DTU. His research interests involve signal detection and estimation, filter design, and image processing.

Christopher S. Ruf (S'85–M'87–SM'92–F'01) received the B.A. degree in physics from Reed College, Portland, OR, and the Ph.D. degree in electrical and computer engineering from the University of Massachusetts, Amherst.

He is currently a Professor of atmospheric, oceanic, and space sciences and electrical engineering and computer science and the Director of the Space Physics Research Laboratory, University of Michigan, Ann Arbor. He has worked previously at Intel Corporation, Hughes Space and Communications, the NASA Jet Propulsion Laboratory, and Pennsylvania State University. In 2000, he was a Guest Professor with the Technical University of Denmark, Lyngby. He has published more than 97 refereed articles in the areas of microwave remote sensing instrumentation and geophysical retrieval algorithms.

Dr. Ruf is a member of the American Geophysical Union (AGU), the American Meteorological Society (AMS), and the Union Radio Scientifique Internationale Commission F. He has served or is serving on the Editorial Boards of the IEEE GRS-S NEWSLETTER, the AGU *Radio Science*, the IEEE TRANSACTIONS ON GEOSCIENCE AND REMOTE SENSING, and the AMS *Journal of Atmospheric and Oceanic Technology*. He was a recipient of three NASA Certificates of Recognition and four NASA Group Achievement Awards, as well as the 1997 GRS-S Transactions Prize Paper Award and the 1999 IEEE Judith A. Resnik Technical Field Award.